Brief Communications

Visual Deprivation During the Critical Period Enhances Layer 2/3 GABAergic Inhibition in Mouse V1

Madhuvanthi Kannan,[1] **Garrett G. Gross,**[2] **Don B. Arnold,**[2] **and Michael J. Higley**[1]

[1]Department of Neuroscience, Program in Cellular Neuroscience, Neurodegeneration, and Repair, Yale University School of Medicine, New Haven, Connecticut 06510, and [2]Department of Biology, University of Southern California, Los Angeles, California 90089

The role of GABAergic signaling in establishing a critical period for experience in visual cortex is well understood. However, the effects of early experience on GABAergic synapses themselves are less clear. Here, we show that monocular deprivation (MD) during the adolescent critical period produces marked enhancement of GABAergic signaling in layer 2/3 of mouse monocular visual cortex. This enhancement coincides with a weakening of glutamatergic inputs, resulting in a significant reduction in the ratio of excitation to inhibition. The potentiation of GABAergic transmission arises from both an increased number of inhibitory synapses and an enhancement of presynaptic GABA release from parvalbumin- and somatostatin-expressing interneurons. Our results suggest that augmented GABAergic inhibition contributes to the experience-dependent regulation of visual function.

Key words: **gephyrin; interneuron; monocular deprivation; optogenetics**

Significance Statement

Visual experience shapes the synaptic organization of cortical circuits in the mouse brain. Here, we show that monocular visual deprivation enhances GABAergic synaptic inhibition in primary visual cortex. This enhancement is mediated by an increase in both the number of postsynaptic GABAergic synapses and the probability of presynaptic GABA release. Our results suggest a contributing mechanism to altered visual responses after deprivation.

Introduction

A general feature of brain development is that heightened periods of experience-dependent plasticity are essential for normal formation of neuronal circuits (Katz and Shatz, 1996; White and Fitzpatrick, 2007; Holtmaat and Svoboda, 2009; Ko et al., 2013). These "critical periods" are shaped by patterns of molecular and cellular activity and are strongly influenced by environmental stimuli. In the rodent visual system, monocular deprivation (MD) during young adolescence leads to degradation of visual acuity (Frenkel and Bear, 2004). Moreover, both monocular and binocular areas of primary visual cortex (V1) respond to MD with a rapid depression of responsiveness to the deprived eye, followed in some cases by a delayed recovery to baseline activity, via mechanisms that are not completely understood (Rittenhouse et al., 1999; Heynen et al., 2003; Frenkel and Bear, 2004; Kaneko et al., 2008; Yoon et al., 2009; Hengen et al., 2013; Keck et al., 2013).

A large body of evidence links maturation of GABAergic synaptic inhibition to the establishment of the visual critical period (Hensch et al., 1998; Fagiolini and Hensch, 2000; Morales et al., 2002; Sale et al., 2010). Mice with transgenic reduction in GABA synthesis fail to exhibit visual critical period onset until triggered by exogenous application of the GABA receptor agonist diazepam (Fagiolini and Hensch, 2000). Interestingly, maturation of inhibition beyond a set point is also thought to contribute to critical period termination because administration of GABA receptor antagonists or a reduction in interneuron activity can reopen the critical period in adult mice (Sale et al., 2007; Harauzov et al., 2010; Kuhlman et al., 2013).

GABAergic circuits themselves are sensitive to experience, although reports differ on the direction of inhibitory changes during visual plasticity across layers and developmental ages. For example, studies of monocular visual cortex have found enhanced perisomatic inhibition onto pyramidal neurons (PNs) in the thalamorecipient layer 4 after critical period MD (Maffei et al., 2006; Nahmani and Turrigiano, 2014). This result is known to

Received Jan. 6, 2016; revised April 11, 2016; accepted April 23, 2016.

Author contributions: M.K., G.G.G., D.B.A., and M.J.H. designed research; M.K. performed research; G.G.G. and D.B.A. contributed unpublished reagents/analytic tools; M.K. analyzed data; M.K. and M.J.H. wrote the paper.

The authors declare no competing financial interests.

The work was supported by the Brain and Behavior Research Foundation (M.J.H.), the Klingenstein Foundation (M.J.H.), the March of Dimes (M.J.H.), and the National Institutes of Health (Grant MH099045 to M.J.H. and Grant NS081678 to D.B.A.). We thank Jess Cardin and members of the Higley laboratory for comments during the preparation of this manuscript.

Correspondence should be addressed to Michael J. Higley, Department of Neuroscience, Program in Cellular Neuroscience, Neurodegeneration, and Repair, Yale University School of Medicine, BCMM 454E, 295 Congress Ave., New Haven, CT 06510. E-mail: m.higley@yale.edu.

DOI:10.1523/JNEUROSCI.0051-16.2016

 0270-6474/16/365914-06$15.00/0

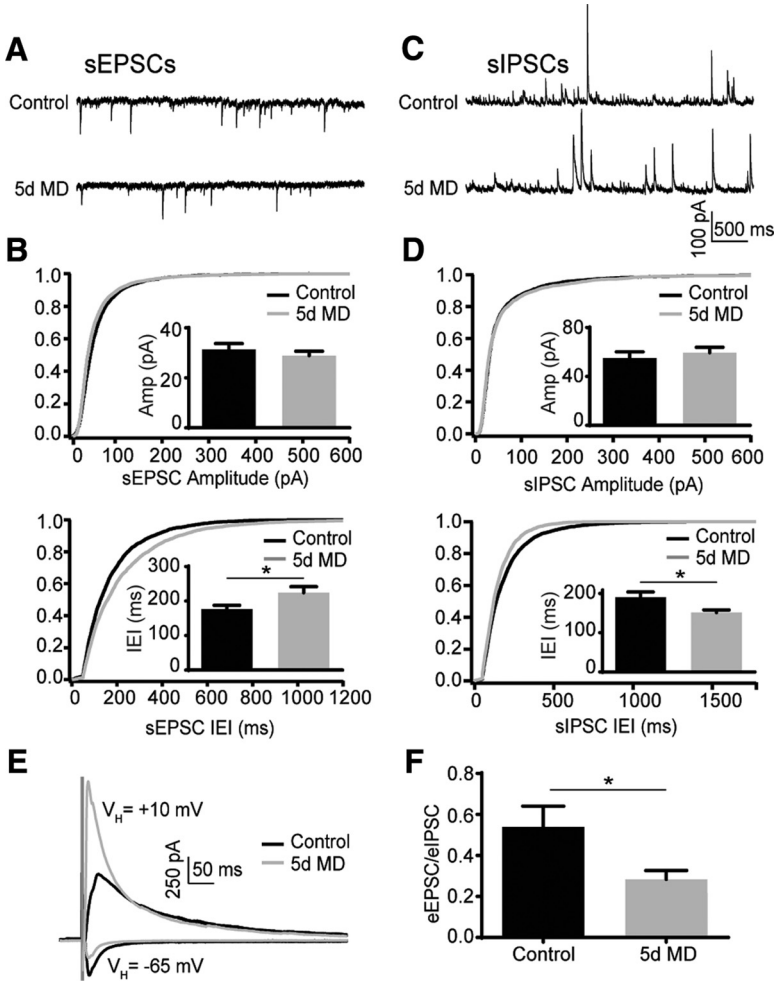

Figure 1. MD decreases the excitation/inhibition ratio in layer 2/3 PNs. ***A***, Example traces of sEPSC recordings for control and 5 d MD conditions. ***B***, Cumulative distribution of sEPSC amplitudes (top) and interevent intervals (bottom) for control (black) and 5 d MD (gray). Insets, mean (±SEM) sEPSC amplitude (top) and interevent interval (bottom) for control (black) and 5 d MD (gray). *$p < 0.05$. ***C***, Example traces of sIPSC recordings for control and 5 d MD conditions. ***D***, Cumulative distribution of sIPSC amplitudes (top) and interevent intervals (bottom) for control and 5 d MD. Insets, mean (±SEM) sIPSC amplitude (top) and interevent interval (bottom) for control (black) and 5 d MD (gray). *$p < 0.05$. ***E***, Example traces of eIPSCs and eEPSCs for control (black) and 5 d MD (gray). ***F***, Mean (±SEM) eEPSC/eIPSC ratio for control (black) and 5 d MD (gray) conditions. *$p < 0.05$.

decrease excitatory drive to layer 2/3 (Maffei and Turrigiano, 2008), potentially leading to a homeostatic reduction in GABAergic inhibition. Indeed, MD in adult animals decreases the number of GABAergic synapses onto the dendrites of layer 2/3 PNs (Chen et al., 2011; van Versendaal et al., 2012), suggesting differences in experience-dependent inhibitory plasticity across layers. Nevertheless, it remains unknown exactly how GABAergic synapses onto layer 2/3 PNs are altered by MD during adolescence.

In the present study, we investigated how MD during the critical period alters GABAergic inhibition in layer 2/3 of the mouse monocular V1. By applying a range of techniques, including electrophysiology and anatomical mapping of GABAergic synapses, we find that reduced visual input leads to a significant increase in GABAergic innervation of layer 2/3 PNs. This increase occurs alongside a weakening of glutamatergic input, significantly reducing the balance of excitation and inhibition. The enhanced GABAergic input arises in part from an increase in the number of inhibitory synapses formed onto PN dendrites. In addition, MD produces an enhancement of GABA release from both parvalbumin-expressing interneurons (PV-INs) and somatostatin-expressing interneurons (SOM-INs). Overall, our results suggest that the augmentation of GABAergic inhibition plays a role in the modulation of visual responses after critical period visual deprivation.

Materials and Methods

MD. All animal handling was done according to the Yale Institutional Animal Care and Use Committee and federal guidelines. Subjects comprised C57BL/6, SOM-Cre, and PV-Cre (Hippenmeyer et al., 2005; Taniguchi et al., 2011) mice of both sexes. Monocular eyelid suture was performed at postnatal day 23 (P23), P25, or P27 and was maintained until P28. For suturing, animals were maintained under 1–2% isoflurane anesthesia. The area surrounding the right eye was cleaned with alcohol swabs and a few drops of saline were administered to keep the eye moist during the procedure. Artificial tears were applied to the left, nonsutured eye to prevent drying. Eyelashes were trimmed and the eyelids were closed with four mattress sutures using 7-0 polyester (Ethicon). The sutures were opened and eyes were examined before electrophysiological or histological analyses. Animals that developed cataracts were discarded from further analyses.

ChR2 expression and activation. To stimulate PV- or SOM-expressing interneurons, PV-Cre or SOM-Cre mice were intracranially injected at P14–P16 in the left V1 with recombinant adeno-associated virus encoding Cre-dependent ChR2-EYFP fusion protein [AAV-DIO-EF1α-ChR2(H134R)-EYFP; Zhang et al., 2006; UNC Vector Core]. Injected mice were killed at P28 for slice physiology, as described below. To activate ChR2-positive fibers optically, the back aperture of the microscope objective (60×, 1.0 numerical aperture) was overfilled with collimated blue light from a fiber-coupled 473 nm laser. Laser activation resulted in an ~15- to 20-μm-diameter disc of light at the focal plane centered on the field of view. A brief pulse (0.5–1 ms) of light (0.5 to 2 mW at the sample) evoked IPSCs reliably in postsynaptic PNs. Trials included single and paired pulses with an interstimulus interval of 100 ms and an intertrial interval of 10 s.

In utero *electroporation, histology, and confocal imaging.* To determine inhibitory synaptic localization, a plasmid encoding the GFP-tagged gephyrin-targeting intrabody FingR (fibronectin intrabody generated by mRNA display; Gross et al., 2013) was electroporated into embryonic day 15 (E15) wild-type C57BL/6 mice embryos *in utero* (Kwon et al., 2012). An E15 pregnant dam was anesthetized using 2% isoflurane and injected intraperitoneally with 0.1 mg/kg fentanyl. The intact uterus containing the embryos was temporarily removed from the abdomen. The embryos were each injected into the left ventricle with 1 μl of DNA mixture containing 1 μg of pCAG-GPHN.FingR plasmid and 0.5 μg of pCAG-dsRED plasmid (Addgene, #11151) using an ~30-μm-diameter pipette sharply beveled at 15°–20°. Injection was visualized using 0.005% Fast Green dye, which was added to the DNA solution. To target transfection of monocular (medial) V1, the positive electrode was placed above and behind the left cortical hemisphere and the negative electrode near the snout. Brief electric pulses (5 × 50 ms/45 V) were delivered using a BTX–Harvard Apparatus ECM 830 Square Wave electroporator. After electroporation, the intact uterus was returned to the abdomen and the mother's abdominal wall and skin were sutured shut.

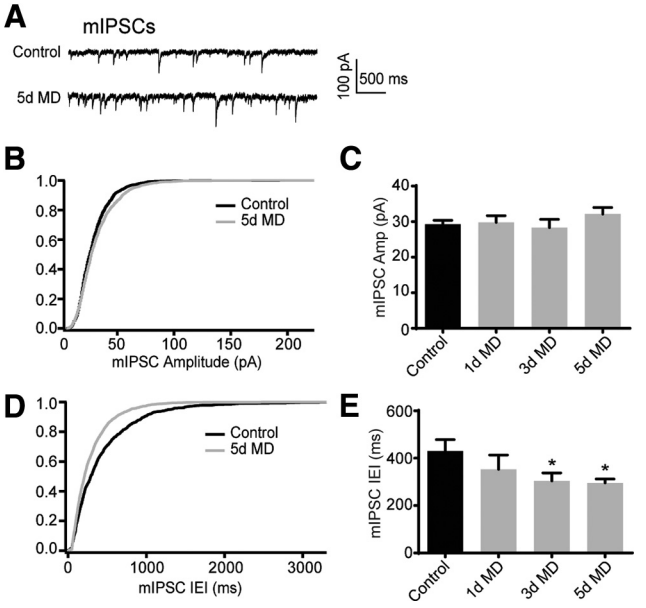

Figure 2. MD decreases the mIPSC interevent interval but not amplitude. ***A***, Example traces of mIPSC recordings for control and 5 d MD conditions. ***B***, Cumulative distribution of mIPSC amplitudes for control (black) and 5 d MD (gray) conditions. ***C***, Mean (±SEM) mIPSC amplitude for control (black) and 1 d, 3 d, and 5 d MD (gray) conditions. *$p < 0.05$. ***D***, ***E***, Same as ***B*** and ***C*** but for the mIPSC interevent interval.

At P28, control and sutured electroporated mice were transcardially perfused with ice-cold PBS followed by 4% PFA (Electron Microscopy Sciences). Brains were postfixed in 4% PFA for 2–3 h at 4°C and 40 μm slices of the transfected left hemisphere were prepared using a vibratome (Leica). The sections were mounted on gelatin-coated glass microscope slides using ProlongGold (Invitrogen). Confocal images of transfected, layer 2/3 PNs of V1 were obtained using a Zeiss 710 confocal microscope with a 63× oil-immersion objective. Gephyrin puncta, corresponding to putative GABAergic synapses along randomly selected apical dendrites, were quantified using ImageJ and the MATLAB-based program SynD (Schmitz et al., 2011). First, the background green channel (GPHN-FingR) puncta were subtracted from each *Z*-stack using ImageJ. The red channel (dsRed) image was converted to a binary mask and each pixel was multiplied with the corresponding pixel from the green channel to identify puncta that belonged on the mask. The spatial distribution of the puncta was then quantified using SynD. Synapse size was set at 0.2 μm and neurite padding (synapse displacement from neurite) at 0.5 μm. Total gephyrin puncta density was quantified as the number of GFP-positive puncta per micrometer length of dendrite in control and deprived conditions. Gephyrin puncta distribution along the somato-dendritic axis was obtained by plotting the density of gephyrin-positive puncta (5 μm bins) as a function of distance from the soma.

Slice preparation. Under isoflurane anesthesia, mice were decapitated and transcardially perfused with ice-cold choline-artificial CSF (choline-ACSF) containing the following (in mM): 110 choline, 25 $NaHCO_3$, 1.25 NaH_2PO_4, 2.5 KCl, 7 $MgCl_2$, 0.5 $CaCl_2$, 20 glucose, 11.6 sodium ascorbate, and 3.1 sodium pyruvate. Acute occipital slices (300 μm) were prepared from the left hemisphere and transferred to ACSF solution containing the following (in mM): 127 NaCl, 25 $NaHCO_3$, 1.25 NaH_2PO_4, 2.5 KCl, 1 $MgCl_2$, 2 $CaCl_2$, and 20 glucose bubbled with 95% O_2 and 5% CO_2. After an incubation period of 30 min at 32°C, the slices were maintained at room temperature until use.

Electrophysiology. Visualized patch-clamp recordings were performed by targeting layer 2/3 PNs in the monocular region of V1. All recordings were performed at 32°C. Criteria for recording included a series resistance (R_s) of <30 MΩ and an input resistance between 100 and 200 MΩ. R_s values are presented for each group in the Results section. Spontaneous and evoked inhibitory currents were recorded by holding cells in voltage clamp at the reversal potential for glutamatergic currents (+10 mV); excitatory currents were obtained at the reversal potential for $GABA_A$-mediated currents (−65 mV). Electrically evoked responses were obtained with extracellular stimulation in layer 2/3 using a bipolar tungsten electrode placed 100–150 μm lateral from the recorded cell. For evoked responses, the ACSF was adjusted to contain 2 mM $CaCl_2$ and 2 mM $MgCl_2$. For miniature inhibitory current recordings, the ACSF also contained 1 μM TTX, 10 μM CPP, and 10 μM NBQX to block sodium channels, NMDA-type, and AMPA-type glutamate receptors, respectively. For most experiments, the internal solution contained the following (in mM): 126 cesium gluconate, 10 HEPES, 10 sodium phosphocreatine, 4 $MgCl_2$, 4 Na_2ATP, 0.4 Na_2GTP, and 1 EGTA, pH 7.3 with CsOH. For recording inward miniature inhibitory currents, cesium chloride was substituted for cesium gluconate up to a concentration of 100 mM and cells were held at −65 mV.

Analysis. Custom-written algorithms in Igor Pro (Wavemetrics) were used to detect and measure spontaneous and miniature events based on a template-matching method (Clements and Bekkers, 1997). For evoked responses, synaptic amplitude was calculated as the peak of the response. The E/I ratio was computed as the ratio of the peak excitatory to inhibitory current. Statistical analyses consisted of *t* tests with Welch's correction for the data shown in Figures 1, 2, and 3 and Mann–Whitney tests for the data shown in Figure 4 due to non-normally distributed data.

Results

To understand how sensory experience impacts GABAergic inhibition, we prepared acute slices of V1 from P28 mice deprived of monocular vision between P23 and P28. First, we evaluated synaptic inputs to layer 2/3 PNs contralateral to the deprived eye. Spontaneous EPSCs and IPSCs (sEPSCs and sIPSCs, respectively) were obtained by voltage-clamping cells at the reversal potential for GABAergic (−65 mV) and glutamatergic (+10 mV) synapses, respectively. Five days of MD did not alter the amplitude of either excitatory (31.37 ± 2.36 pA, $n = 10$ cells, $R_s = 14.83 \pm 1.6$ MΩ vs 28.88 ± 1.76 pA, $n = 12$ cells, $R_s = 13.15 \pm 0.76$ MΩ, $p = 0.41$, unpaired *t* test with Welch's correction) or inhibitory (54.98 ± 5.13 pA, $n = 17$ cells, $R_s = 16.32 \pm 1.5$ MΩ vs 59.41 ± 4.42 pA, $n = 12$ cells, $R_s = 15.92 \pm 1.0$ MΩ, $p = 0.52$) currents. However, MD increased the interevent interval of sEPSCs significantly from 176.3 ± 11.27 ms to 224.2 ± 17.29 ms ($p = 0.032$). Surprisingly, MD also decreased the interevent interval of sIPSCs from 190.3 ± 13.49 ms to 151.4 ± 6.68 ms ($p = 0.017$; Fig. 1*A–D*).

To further characterize the impact of MD on the balance of excitation and inhibition in individual cells, we evoked excitatory EPSCs and IPSCs (eEPSCs and eIPSCs, respectively) by local electrical stimulation, voltage-clamping individual neurons at −65 mV and +10 mV, respectively. The mean E/I ratio for evoked responses was reduced significantly by MD (0.28 ± 0.04, $n = 12$ cells, $R_s = 18.9 \pm 1.0$ MΩ) compared with controls (0.54 ± 0.1, $n = 9$ cells, $R_s = 19.52 \pm 1.8$ MΩ, $p = 0.041$; Fig. 1*E*,*F*). The average amplitude of eEPSCs did not differ between the two groups (250.9 ± 39.31 pA vs 254.8 ± 43.45 pA, $p = 0.95$). However, the eIPSCs were increased significantly under deprivation relative to controls (587.0 ± 140.6 pA vs 1019.0 ± 152.3 pA, $p = 0.05$, data not shown).

To determine whether the increased sIPSC frequency reflects enhanced GABAergic synaptic innervation of layer 2/3 PNs, we next measured the amplitude and frequency of activity-independent miniature IPSCs (mIPSCs) in the presence of the sodium channel blocker TTX (Fig. 2*A*). For mIPSCs, mice were sutured at P23, P25, or P27 and slices were prepared at P28. In all three groups, MD did not affect mIPSC amplitude (control: 29.24 ± 1.13 pA, $n = 14$ cells, $R_s = 15.68 \pm 0.6$ MΩ; 1 d MD: 29.83 ± 1.86 pA, $n = 10$ cells, $R_s = 14.94 \pm 0.83$ MΩ, $p = 0.79$; 3 d MD: 28.34 ± 2.31, $n = 9$ cells, $R_s = 15.47 \pm 0.86$ MΩ, $p =$

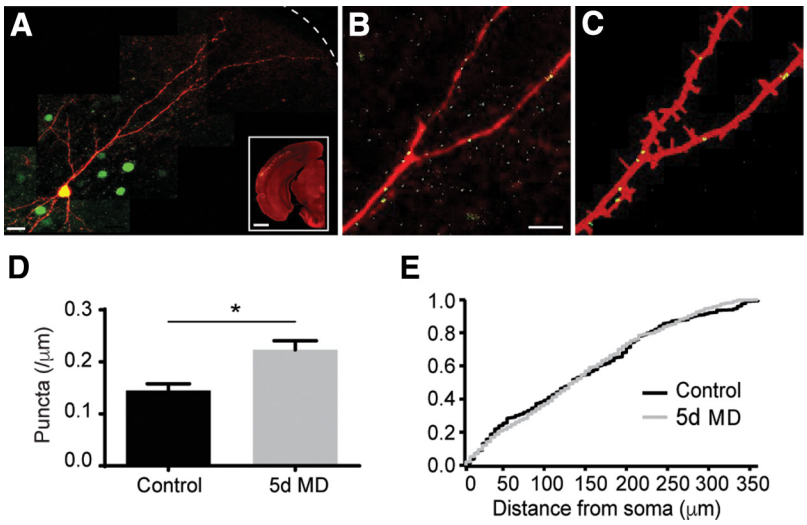

Figure 3. MD increases gephyrin puncta density in apical dendrites of layer 2/3 PNs. ***A***, dsRED-express (red) and GPHN.FingR staining (green) along the somatodendritic axis of a layer 2/3 PN. Dashed line indicates pial surface. Scale bar, 10 μm. Inset, *In utero* electroporation of layer 2/3 PNs of mouse V1. Scale bar, 1 mm. ***B***, Magnified view of a fragment of the neuron in ***A***. Scale bar, 5 μm. ***C***, Calculated neurite mask (red) and identified gephyrin puncta (green) for the neuronal fragment in ***B***. ***D***, Mean (±SEM) gephyrin puncta density along apical dendrites in control (black) and 5 d MD (gray) conditions. *$p < 0.05$. ***E***, Cumulative distribution of gephyrin puncta along the somatodendritic axis in control (black) and 5 d MD (gray).

0.73; 5 d MD: 32.15 ± 1.85 pA, $n = 18$ cells, $R_s = 14.18 \pm 0.77$ MΩ, $p = 0.19$; Fig. 2*B*,*C*). However, MD produced a significant decrease in the mIPSC interevent interval (control: 430.0 ± 47.99 ms; 1 d MD: 353.4 ± 59.74 ms, $p = 0.33$; 3 d MD: 304.2 ± 33.52 ms, $p = 0.044$; 5 d MD: 295.6 ± 16.61 ms, $p = 0.018$; Fig. 2*D*,*E*). Overall, these data are consistent with either an increased number of GABAergic synapses or increased presynaptic release.

To further investigate whether MD increases the number of inhibitory synapses, we used a recombinant, antibody-like protein (GPHN.FingR) to label fluorescently endogenous gephyrin (Gross et al., 2013), a postsynaptic scaffolding molecule associated with GABAergic synapses (Craig et al., 1996; Tretter et al., 2008; Tretter et al., 2012). We used *in utero* electroporation to express the GFP-tagged GPHN.FingR and a cytosolic red fluorophore dsRED-express in layer 2/3 PNs. GPHN.FingR thus allowed the visual detection of putative GABAergic synapses (Fig. 3*A*–*C*). For this analysis, mice were deprived at P23 and cells were analyzed at P28. MD increased the average gephyrin puncta density in the apical dendrites significantly from 0.145 ± 0.013/μm ($n = 7$ cells) to 0.223 ± 0.017/μm ($n = 9$ cells, $p = 0.0029$; Fig. 3*D*). The density of puncta was uniformly increased along the somato-dendritic axis (Fig. 3*E*). These results support the conclusion that MD increases the number of GABAergic synapses throughout the apical dendritic arbor.

Finally, we investigated whether MD also produces changes in presynaptic GABA release from identified inhibitory interneurons. We expressed the light-activated cation channel channelrhodopsin-2 (ChR2) in either PV-INs or SOM-INs. In acute slices of V1, brief light pulses (0.5–1 ms, 473 nm) caused eIPSCs. To assess presynaptic release, we quantified the paired pulse ratio (PPR, 100 ms interval) for eIPSCs. MD (P23–P28) produced a significant decrease in the PPR for PV-IN-mediated eIPSCs from 2.04 ± 0.59 ($n = 8$ cells, $R_s = 16.8 \pm 1.4$ MΩ) to 0.76 ± 0.049 ($n = 6$ cells, $R_s = 28.7 \pm 2.0$ MΩ, $p = 0.0047$, Mann–Whitney test; Fig. 4*A*–*C*). The surprising facilitation of PV-IN-mediated eIPSCs in the control group may be due to the expression of ChR2 in a heterogeneous population of PV-positive interneurons. MD also produced a significant decrease in PPR for SOM-IN-mediated eIPSCs from 1.76 ± 0.62 ($n = 8$ cells, $R_s = 20.2 \pm 1.9$ MΩ) to 0.76 ± 0.07 ($n = 10$ cells, $R_s = 28.9 \pm 1.8$ MΩ, $p = 0.0031$; Fig. 4*D*–*F*). Together, these findings suggest that MD also produces an enhancement of presynaptic GABA release from multiple classes of interneurons.

Discussion

GABAergic transmission is pivotal to the opening and closing of the visual critical period (Hensch et al., 1998; Fagiolini and Hensch, 2000; Morales et al., 2002; Sale et al., 2010). However, how GABAergic synapses are themselves altered by visual experience remains less well understood. Here, we show in the mouse that MD during the adolescent critical period (P23–P28) strengthens GABAergic input to layer 2/3 PNs while simultaneously attenuating glutamatergic input. This result is associated with a net decrease in the ratio of electrically evoked excitation to inhibition. Both electrophysiological and anatomical data support the conclusion that enhanced inhibition is primarily due to an increase in the number of GABAergic synapses formed onto individual PNs. However, our data also suggest that MD produces an increase in release probability from both SOM-INs and PV-INs in V1, further elevating the impact of GABAergic signaling.

Our findings are consistent with previous work examining layer 4 PNs, in which visual deprivation during the critical period enhances the amplitude of IPSCs mediated by fast-spiking (presumed PV-expressing) interneurons (Maffei et al., 2006). Indeed, within layer 4, the strengthening of GABAergic transmission is mediated by an increase in postsynaptic GABA-receptor density, as well as by an increase in the density of readily releasable vesicles at interneuron terminals (Nahmani and Turrigiano, 2014; Petrini et al., 2014). Previous work has also shown that multiday MD produced by lid suturing results in a decrease in the ratio of excitation to inhibition within layer 2/3 (Maffei and Turrigiano, 2008). Although this prior study attributed the change primarily to a weakening of excitatory glutamatergic inputs, our results suggest that enhanced GABAergic input also plays a role. Notably, brief (1 d) MD results in weakening of excitation onto PV-INs that would potentially counteract the enhanced GABAergic output, leading to a disinhibited circuit (Kuhlman et al., 2013). However, whether inputs to PV-INs are altered after prolonged deprivation is less clear.

Surprisingly, our data differ from studies conducted in adult animals, in which MD accelerated the loss of inhibitory synapses on layer 2/3 PNs labeled by expression of fluorescently tagged gephyrin (Chen et al., 2012; van Versendaal et al., 2012). Here, we labeled endogenous gephyrin using GFP-tagged GPHN.FingR, an approach previously shown to identify functional synapses (Gross et al., 2013). The discrepancy between these two results may reflect the different labeling strategies or may suggest the intriguing hypothesis that experience has markedly different consequences for cortical circuitry depending on the age of the animal.

Finally, *in vivo* studies show that MD during the critical period initially leads to reduced cortical responses to stimula-

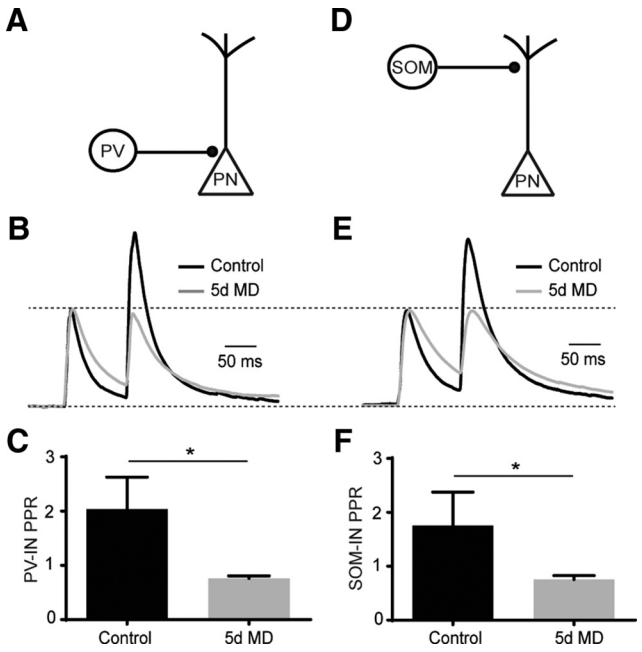

Figure 4. MD increases presynaptic GABA release from PV-INs and SOM-INs. ***A***, Schematic of optogenetic stimulation of ChR2-expressing PV-INs. ***B***, Average, normalized traces of evoked IPSC recordings after paired, optogenetic stimulation of PV-INs in control (black) and 5 d MD (gray). ***C***, Mean (±SEM) PPR of optically evoked responses for control (black) and 5 d MD (gray) conditions. $*p < 0.05$. ***D***, Schematic of optogenetic stimulation of ChR2-expressing SOM-INs. ***E***, Average, normalized traces of evoked IPSC recordings after paired, optogenetic stimulation of SOM-INs in control (black) and 5 d MD (gray). ***F***, Mean (±SEM) PPR of optically evoked responses for control (black) and 5 d MD (gray) conditions. $*p < 0.05$.

tion of the deprived eye, followed by recovery to baseline levels after several days (Frenkel and Bear, 2004; Kaneko et al., 2008; Hengen et al., 2013). The mechanisms underlying these changes are not fully understood, although our results suggest that a rapid increase in GABAergic inhibition may contribute to the early reduction of visually evoked activity. Subsequent restoration of activity appears to involve homeostatic enhancement of excitatory synapses onto both superficial and deep layer PNs (Hengen et al., 2013; Keck et al., 2013; Lambo and Turrigiano, 2013). Interestingly, our data using mice reveal a reduction in spontaneous excitation after 5 d of deprivation, reminiscent of the similar decrease seen in rats for shorter duration lid suture (Maffei and Turrigiano, 2008; Hengen et al., 2013; Lambo and Turrigiano, 2013), suggesting subtle differences in the timing of synaptic modification between the two species. Overall, these findings suggest that the reorganization of visual circuits after MD requires a complex interplay of synaptic excitation and inhibition.

References

Chen JL, Lin WC, Cha JW, So PT, Kubota Y, Nedivi E (2011) Structural basis for the role of inhibition in facilitating adult brain plasticity. Nat Neurosci 14:587–594. CrossRef Medline

Chen JL, Villa KL, Cha JW, So PT, Kubota Y, Nedivi E (2012) Clustered dynamics of inhibitory synapses and dendritic spines in the adult neocortex. Neuron 74:361–373. CrossRef Medline

Clements JD, Bekkers JM (1997) Detection of spontaneous synaptic events with an optimally scaled template. Biophys J 73:220–229. CrossRef Medline

Craig AM, Banker G, Chang W, McGrath ME, Serpinskaya AS (1996) Clustering of gephyrin at GABAergic but not glutamatergic synapses in cultured rat hippocampal neurons. J Neurosci 16:3166–3177. Medline

Fagiolini M, Hensch TK (2000) Inhibitory threshold for critical-period activation in primary visual cortex. Nature 404:183–186. CrossRef Medline

Frenkel MY, Bear MF (2004) How monocular deprivation shifts ocular dominance in visual cortex of young mice. Neuron 44:917–923. CrossRef Medline

Gross GG, Junge JA, Mora RJ, Kwon HB, Olson CA, Takahashi TT, Liman ER, Ellis-Davies GC, McGee AW, Sabatini BL, Roberts RW, Arnold DB (2013) Recombinant probes for visualizing endogenous synaptic proteins in living neurons. Neuron 78:971–985. CrossRef Medline

Harauzov A, Spolidoro M, DiCristo G, De Pasquale R, Cancedda L, Pizzorusso T, Viegi A, Berardi N, Maffei L (2010) Reducing intracortical inhibition in the adult visual cortex promotes ocular dominance plasticity. J Neurosci 30:361–371. CrossRef Medline

Hengen KB, Lambo ME, Van Hooser SD, Katz DB, Turrigiano GG (2013) Firing rate homeostasis in visual cortex of freely behaving rodents. Neuron 80:335–342. CrossRef Medline

Hensch TK, Fagiolini M, Mataga N, Stryker MP, Baekkeskov S, Kash SF (1998) Local GABA circuit control of experience-dependent plasticity in developing visual cortex. Science 282:1504–1508. CrossRef Medline

Heynen AJ, Yoon BJ, Liu CH, Chung HJ, Huganir RL, Bear MF (2003) Molecular mechanism for loss of visual cortical responsiveness following brief monocular deprivation. Nat Neurosci 6:854–862. CrossRef Medline

Hippenmeyer S, Vrieseling E, Sigrist M, Portmann T, Laengle C, Ladle DR, Arber S (2005) A developmental switch in the response of DRG neurons to ETS transcription factor signaling. PLoS Biol 3:e159. CrossRef Medline

Holtmaat A, Svoboda K (2009) Experience-dependent structural synaptic plasticity in the mammalian brain. Nat Rev Neurosci 10:647–658. CrossRef Medline

Kaneko M, Stellwagen D, Malenka RC, Stryker MP (2008) Tumor necrosis factor-alpha mediates one component of competitive, experience-dependent plasticity in developing visual cortex. Neuron 58:673–680. CrossRef Medline

Katz LC, Shatz CJ (1996) Synaptic activity and the construction of cortical circuits. Science 274:1133–1138. CrossRef Medline

Keck T, Keller GB, Jacobsen RI, Eysel UT, Bonhoeffer T, Hübener M (2013) Synaptic scaling and homeostatic plasticity in the mouse visual cortex in vivo. Neuron 80:327–334. CrossRef Medline

Ko H, Cossell L, Baragli C, Antolik J, Clopath C, Hofer SB, Mrsic-Flogel TD (2013) The emergence of functional microcircuits in visual cortex. Nature 496:96–100. CrossRef Medline

Kuhlman SJ, Olivas ND, Tring E, Ikrar T, Xu X, Trachtenberg JT (2013) A disinhibitory microcircuit initiates critical-period plasticity in the visual cortex. Nature 501:543–546. CrossRef Medline

Kwon HB, Kozorovitskiy Y, Oh WJ, Peixoto RT, Akhtar N, Saulnier JL, Gu C, Sabatini BL (2012) Neuroligin-1-dependent competition regulates cortical synaptogenesis and synapse number. Nat Neurosci 15:1667–1674. CrossRef Medline

Lambo ME, Turrigiano GG (2013) Synaptic and intrinsic homeostatic mechanisms cooperate to increase L2/3 pyramidal neuron excitability during a late phase of critical period plasticity. J Neurosci 33:8810–8819. CrossRef Medline

Maffei A, Turrigiano GG (2008) Multiple modes of network homeostasis in visual cortical layer 2/3. J Neurosci 28:4377–4384. CrossRef Medline

Maffei A, Nataraj K, Nelson SB, Turrigiano GG (2006) Potentiation of cortical inhibition by visual deprivation. Nature 443:81–84. CrossRef Medline

Morales B, Choi SY, Kirkwood A (2002) Dark rearing alters the development of GABAergic transmission in visual cortex. J Neurosci 22:8084–8090. Medline

Nahmani M, Turrigiano GG (2014) Deprivation-induced strengthening of presynaptic and postsynaptic inhibitory transmission in layer 4 of visual cortex during the critical period. J Neurosci 34:2571–2582. CrossRef Medline

Petrini EM, Ravasenga T, Hausrat TJ, Iurilli G, Olcese U, Racine V, Sibarita JB, Jacob TC, Moss SJ, Benfenati F, Medini P, Kneussel M, Barberis A (2014) Synaptic recruitment of gephyrin regulates surface GABAA receptor dynamics for the expression of inhibitory LTP. Nat Commun 5:3921. CrossRef Medline

Rittenhouse CD, Shouval HZ, Paradiso MA, Bear MF (1999) Monocular deprivation induces homosynaptic long-term depression in visual cortex. Nature 397:347–350. CrossRef Medline

Sale A, Maya Vetencourt JF, Medini P, Cenni MC, Baroncelli L, De Pasquale

R, Maffei L (2007) Environmental enrichment in adulthood promotes amblyopia recovery through a reduction of intracortical inhibition. Nat Neurosci 10:679–681. CrossRef Medline

Sale A, Berardi N, Spolidoro M, Baroncelli L, Maffei L (2010) GABAergic inhibition in visual cortical plasticity. Front Cell Neurosci 4:10. CrossRef Medline

Schmitz SK, Hjorth JJ, Joemai RM, Wijntjes R, Eijgenraam S, de Bruijn P, Georgiou C, de Jong AP, van Ooyen A, Verhage M, Cornelisse LN, Toonen RF, Veldkamp W (2011) Automated analysis of neuronal morphology, synapse number and synaptic recruitment. J Neurosci Methods 195:185–193. CrossRef Medline

Taniguchi H, He M, Wu P, Kim S, Paik R, Sugino K, Kvitsani D, Fu Y, Lu J, Lin Y, Miyoshi G, Shima Y, Fishell G, Nelson SB, Huang ZJ (2011) A resource of Cre driver lines for genetic targeting of GABAergic neurons in cerebral cortex. Neuron 71:995–1013. CrossRef Medline

Tretter V, Jacob TC, Mukherjee J, Fritschy JM, Pangalos MN, Moss SJ (2008) The clustering of GABA(A) receptor subtypes at inhibitory synapses is facilitated via the direct binding of receptor alpha 2 subunits to gephyrin. J Neurosci 28:1356–1365. CrossRef Medline

Tretter V, Mukherjee J, Maric HM, Schindelin H, Sieghart W, Moss SJ (2012) Gephyrin, the enigmatic organizer at GABAergic synapses. Front Cell Neurosci 6:23. CrossRef Medline

van Versendaal D, Rajendran R, Saiepour MH, Klooster J, Smit-Rigter L, Sommeijer JP, De Zeeuw CI, Hofer SB, Heimel JA, Levelt CN (2012) Elimination of inhibitory synapses is a major component of adult ocular dominance plasticity. Neuron 74:374–383. CrossRef Medline

White LE, Fitzpatrick D (2007) Vision and cortical map development. Neuron 56:327–338. CrossRef Medline

Yoon BJ, Smith GB, Heynen AJ, Neve RL, Bear MF (2009) Essential role for a long-term depression mechanism in ocular dominance plasticity. Proc Natl Acad Sci U S A 106:9860–9865. CrossRef Medline

Zhang F, Wang LP, Boyden ES, Deisseroth K (2006) Channelrhodopsin-2 and optical control of excitable cells. Nat Methods 3:785–792. CrossRef Medline